

# Selective Delivery of Secretory Cargo in Golgi-Derived Carriers of Nonepithelial Cells

Amin Rustom<sup>1,5</sup>, Mark Bajohrs<sup>1,5</sup>,  
Christoph Kaether<sup>1</sup>, Patrick Keller<sup>2,3</sup>,  
Derek Toomre<sup>2</sup>, Denis Corbeil<sup>1,3</sup> and  
Hans-Hermann Gerdes<sup>1,\*</sup>

<sup>1</sup> Department of Neurobiology, Interdisciplinary Center of Neuroscience, University of Heidelberg, INF 364, D-69120 Heidelberg, Germany

<sup>2</sup> European Molecular Biology Laboratory, Cell Biology Programme, D-69012 Heidelberg, Germany

<sup>3</sup> Max-Planck-Institute of Molecular Cell Biology and Genetics, Pfotenhauerstr. 108, D-01307 Dresden, Germany

\* Corresponding author: Hans-Hermann Gerdes, hhgerdes@sun0.urz.uni-heidelberg.de

**In epithelial cells, soluble cargo proteins destined for basolateral or apical secretion are packaged into distinct trans-Golgi network-derived transport carriers. Similar carriers, termed basolateral- and apical-like, have been observed in nonepithelial cells using ectopically expressed membrane marker proteins. Whether these cells are capable of selectively packaging secretory proteins into distinct carriers is still an open question. Here, we have addressed this issue by analyzing the packaging and transport of secretory human chromogranin B fusion proteins using a green fluorescent protein-based high-resolution, dual-color imaging technique. We were able to show that these secretory markers were selectively packaged at the Golgi into tubular/vesicular-like transport carriers containing basolateral membrane markers, resulting in extensive cotransport. In contrast, deletion mutants of the human chromogranin B fusion proteins lacking an N-terminal loop structure were efficiently transported in both basolateral- and apical-like carriers, the latter displaying a spherical morphology. Similarly, in polarized epithelial cells, the human chromogranin B fusion protein was secreted basolaterally and the loop-deleted analogue into both the basolateral and apical medium. These findings suggest that nonepithelial cells, like their epithelial counterparts, possess a sorting machinery capable of selective packaging of secretory cargo into distinct types of carriers.**

**Key words:** green fluorescent protein, multi-color imaging, polarized sorting, trans-Golgi network, transport carriers

Received 29 August 2001, revised and accepted for publication 24 January 2002

In epithelial cells, like Madin-Darby canine kidney (MDCK) cells, most newly synthesized proteins destined for the plasma membrane or for secretion have to be delivered selectively to the apical or basolateral domain of the polarized cell surface. Such proteins are thus packaged at the level of the trans-Golgi network (TGN) into distinct types of transport carriers (1,2). These carriers have been studied mainly by examining membrane proteins such as the basolaterally sorted vesicular stomatitis virus G (VSVG) protein (3,4) or apically sorted glycosylphosphatidylinositol (GPI)-anchored proteins (5) and led to insights into signals and mechanisms involved in their polarized trafficking (6–8). In contrast, the important topic of polarized protein secretion, a prerequisite for proper functioning of tissues and organs, is much less characterized, although the polarized delivery of many proteins has been studied (9–12).

In nonepithelial cells such as fibroblasts, the existence of apical- and basolateral-like carriers has also been reported based on the expression of the same membrane markers, the VSVG protein (13,14) and GPI-anchored proteins (13). However, in these cells the selective delivery of secretory proteins has been poorly addressed to date, although under certain conditions such as cell migration it may be of pivotal importance. Therefore it is not known whether e.g. basolateral- and apical-like carriers also selectively transport soluble proteins destined for secretion. We have previously monitored protein secretion of nonepithelial Vero cells by labeling the respective post-Golgi transport carriers using transfection of a fusion protein consisting of human chromogranin B (hCgB) and green fluorescent protein (GFP) (15). Although the hCgB fusion protein was shown to serve as an efficient secretory marker protein (15), this single color analysis did not allow us to examine transport selectivity. We here investigated the transport selectivity of hCgB fusion proteins by analyzing their correlative transport dynamics together with membrane protein markers of basolateral- and apical-like carriers. This was achieved by using a GFP-based high-resolution dual-color imaging technique (16). Our results show that Vero cells like polarized epithelial cells, possess a sorting machinery capable of selective packaging of secretory cargo into distinct constitutive carriers. In addition, we show that in both cell types a defined loop structure of hCgB (17) is essential for basolateral and basolateral-like targeting of this fusion protein.

## Results

### *Human chromogranin B-enhanced yellow fluorescent protein is a soluble marker protein employed to monitor constitutive secretory vesicles*

In order to visualize post-Golgi transport carriers of nonepithelial cells transporting soluble cargo, we transfected Vero

<sup>5</sup> A.R. and M.B. contributed equally.

cells with a fusion protein consisting of hCgB and enhanced yellow fluorescent protein (EYFP). Videomicroscopic analysis revealed that the fluorescence signals of hCgB-EYFP transport carriers displayed a punctuated appearance (see below) consistent with previous observations obtained with a similar fusion protein (15). With an apparent diameter of approximately 450 nm, these fluorescence signals suggested a spherical morphology of the respective carriers (see below). Rarely, chains composed of individual signals showed concerted movement as if they were lined up within invisible, i.e. nonfluorescent, tubular carriers (not shown). It is conceivable that the spherical appearance of hCgB-EYFP carriers is caused or accentuated by its aggregative (18) properties.

#### **Human chromogranin B-enhanced yellow fluorescent protein is transported in basolateral-like carriers**

First we addressed whether carriers transporting hCgB-EYFP were identical with basolateral- and/or apical-like carriers so far identified in nonepithelial cells. We therefore coexpressed hCgB-EYFP and VSVG fused via a spacer sequence to enhanced cyan fluorescent protein (ECFP) which has recently been shown to serve as a specific membrane marker for basolateral-like carriers (19). We exploited the temperature-dependent retention of VSVG-ECFP in the endoplasmic reticulum at 39.5°C followed by a 20°C secretion block (20) to selectively accumulate both markers in the TGN (Figure 1a, asterisk). Reversal of the secretion block at 37°C in the presence of cycloheximide followed by dual-color videomicro-

scopy permitted monitoring of Golgi-derived transport carriers positive for hCgB-EYFP (Figure 1, red) and VSVG-ECFP (Figure 1, green) en route to the plasma membrane. Many of these carriers were positive for both markers, as indicated by the yellow color (Figure 1b<sub>1</sub>, arrows) in the overlay of the single channel recordings. Those carriers containing exclusively VSVG-ECFP (Figure 1b<sub>1</sub>, open arrowheads) may be indicative of a higher expression level for VSVG-ECFP as compared to hCgB-EYFP. A quantitative analysis of colocalization for the observed time period, referred to here as dynamic colocalization, was performed assisted by fully automated object detection (Figure 1b<sub>2</sub>) and particle tracking (Figure 1c) (for details, see Methods). This showed that  $71.2\% \pm 11.5$  SD ( $n=9$  cells of 3 independent experiments) of hCgB-EYFP positive structures also contained VSVG-ECFP (Figure 1b<sub>2</sub>,c, yellow). Interestingly, for many of them, the fluorescence signals were slightly displaced with respect to one another, resulting in a double-spherical appearance (Figure 1b<sub>1</sub>, open arrow, see below). Collectively, these data show that the secretory marker hCgB-EYFP is efficiently cotransported with VSVG-ECFP in basolateral-like carriers.

#### **Human chromogranin B-enhanced yellow fluorescent protein is excluded from apical-like carriers**

To evaluate whether the cotransport of hCgB-EYFP and VSVG-ECFP is selective, we analyzed the colocalization of hCgB-EYFP with glycosylphosphatidylinositol (GPI)-anchored

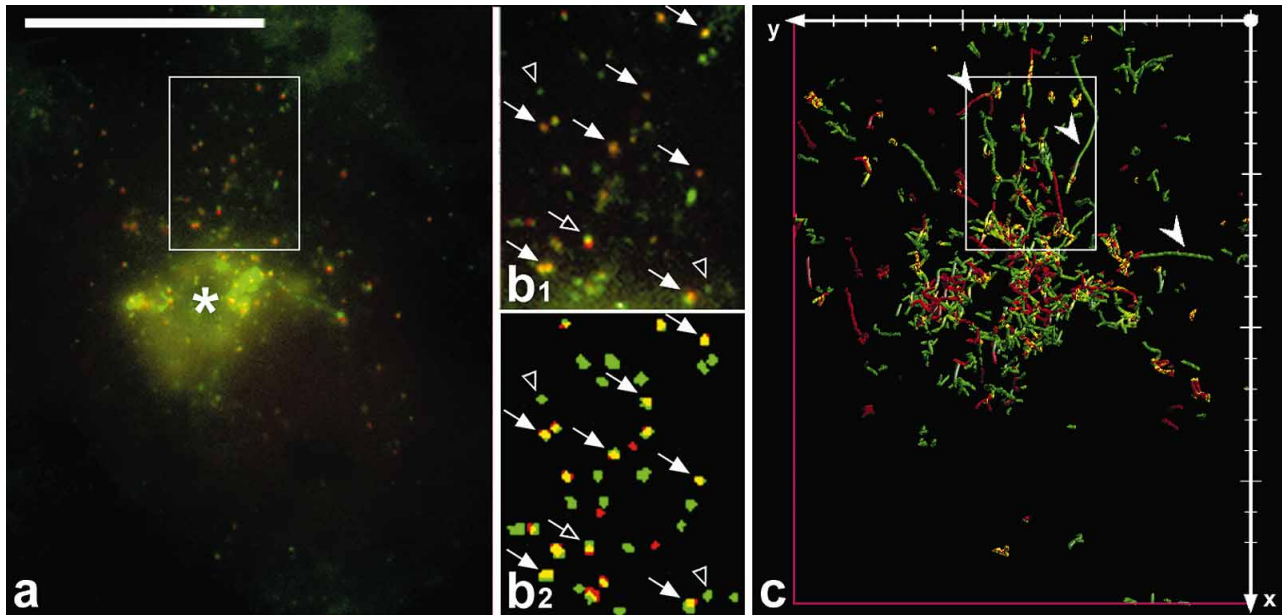


**Figure 1: Transport of secretory cargo in basolateral-like carriers.** Vero cells were cotransfected with hCgB-EYFP (red) and VSVG-ECFP (green). Note that yellow indicates colocalization of both markers. Cells were prepared for imaging as described (see Methods). Colocalization was analyzed for the boxed area in (a) magnified in (b<sub>1</sub>). The asterisk in (a) indicates the Golgi region. Automated object detection (b<sub>2</sub>) and tracking (c) were performed (see Methods). Representative non-colocalizing (arrowheads) and colocalizing structures (arrows) are indicated in (b<sub>1</sub>, b<sub>2</sub>), respectively. Open arrowheads indicate VSVG-positive structures negative for hCgB-EYFP. Open arrow indicates an object with shifted fluorescence signals. For the cell depicted in (a), a track display of automatically detected objects is shown (c). Barbed arrowheads indicate long-range transport of basolateral-like carriers. The boxed area in (c) corresponds to the box in (a). Scale bar, 20  $\mu$ m. An entire movie covering 15.8 s can be viewed in the video gallery in the Traffic web site at [www.traffic.dk](http://www.traffic.dk).

ECFP (GPI-ECFP), a membrane marker for apical-like carriers (19). Prior to imaging, Vero cells cotransfected with hCgB-EYFP and GPI-ECFP were incubated with phosphatidylinositol phospholipase C (PI-PLC) during the 20°C secretion block to release GPI-anchored ECFP from the cell surface, thus permitting the visualization of the Golgi (Figure 2a, asterisk) and Golgi-derived transport carriers positive for hCgB-EYFP (Figure 2, red) and GPI-ECFP (Figure 2, green). A computer-assisted, quantitative analysis of dynamic colocalization was performed as described (Figure 2b<sub>2</sub>,c). In contrast to the extensive colocalization of hCgB-EYFP-positive structures with VSVG-ECFP, only 17.6% ± 11.1 SD (n = 9 cells of 3 independent experiments) of these structures also contained GPI-ECFP (Figure 2b<sub>1</sub>,b<sub>2</sub>, arrows). We do not believe that this difference is due to the 39.5°C secretion block used to analyze VSVG-ECFP, since similar results were obtained without this temperature block (not shown). In addition, it is highly unlikely that the absence of hCgB-EYFP signals in apical-like carriers was caused by a loss in fluorescence due to specific milieu conditions because EYFP and ECFP as such were both fluorescent in apical- and basolateral-like carriers (not shown). Together, these data indicate that hCgB-EYFP is largely excluded from apical-like carriers and is predominantly transported in basolateral-like carriers. This finding corresponds with our observation in polarized epithelial cells that a similar fusion protein, hCgB-GFP(S65T) (20), when expressed in stably transfected MDCK cells, was secreted to 80% ± 5.5 SD (n = 3 independent experiments) into the

basolateral medium. It is noteworthy that these results indicate conspicuous similarities of transport selectivity between the two cell systems.

#### ***A deletion mutant of hCgB-EYFP is transported in both basolateral- and apical-like carriers***

What determines the selective transport of hCgB-EYFP in basolateral types of carriers? To address this question, we used mutants of this fusion protein lacking the N-terminal disulfide-bonded loop of hCgB, previously identified as a sorting signal directing soluble cargo to the regulated pathway of protein secretion in neuroendocrine cells (17). To analyze a potential influence of this structural domain for selective transport in nonepithelial Vero cells, we expressed the loop-deleted fusion protein, Δcys-hCgB-EYFP together with basolateral- and apical-like marker proteins and analyzed their colocalization as already performed for hCgB-EYFP. Remarkably, the loop-deleted Δcys-hCgB-EYFP (Figure 3, red) colocalized to 60.4% ± 6.6 SD (n = 9 cells of 3 independent experiments) (Figure 3a<sub>1</sub>,a<sub>2</sub>, arrows) with the apical-like marker protein GPI-ECFP (Figure 3a<sub>1</sub>,a<sub>2</sub>, green), contrasting the explicit exclusion of hCgB-EYFP from the respective type of carrier. The colocalization of Δcys-hCgB-EYFP and VSVG-ECFP (Figure 3b<sub>1</sub>,b<sub>2</sub>, green) was found to be 83.8% ± 7.4 SD (n = 9 of 3 independent experiments), thus in the same range as observed for hCgB-EYFP and VSVG-ECFP (Figure 3b<sub>1</sub>,b<sub>2</sub>, arrows).

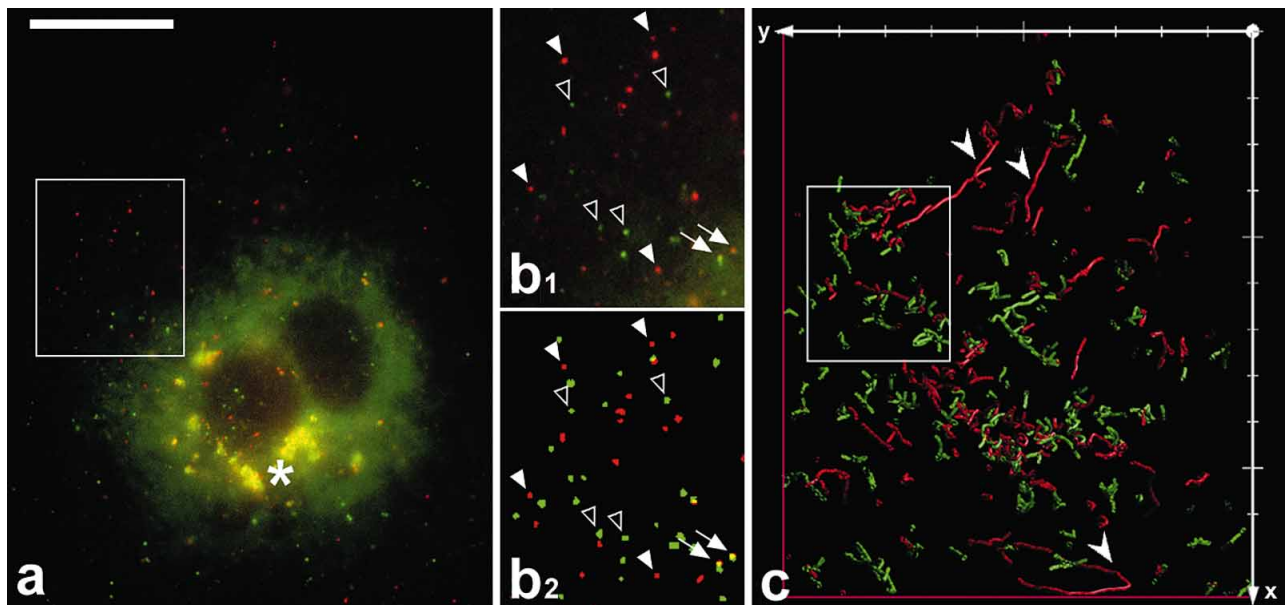


**Figure 2: Exclusion of hCgB-EYFP from apical-like carriers.** Vero cells were cotransfected with hCgB-EYFP (red) and GPI-ECFP (green). Note that yellow indicates colocalization of both markers. Cells were prepared for imaging as described in Methods. Colocalization was analyzed for the boxed area in (a) magnified in (b<sub>1</sub>). The asterisk in (a) indicates the Golgi region. Automated object detection (b<sub>2</sub>) and tracking (c) were performed (see Methods). In the middle panels, representative non-colocalizing (arrowheads) and colocalizing structures (arrows) are indicated. Filled arrowheads indicate hCgB-positive structures. Open arrowheads indicate VSVG-positive structures. For the cell depicted in (a), a track display of automatically detected objects is shown (c). Barbed arrowheads indicate long-range transport of basolateral-like carriers. The boxed area in (c) corresponds to the box in (a). Scale bar, 20 μm. An entire movie covering 21.6 s can be viewed in the video gallery at the Traffic web site at [www.traffic.dk](http://www.traffic.dk).

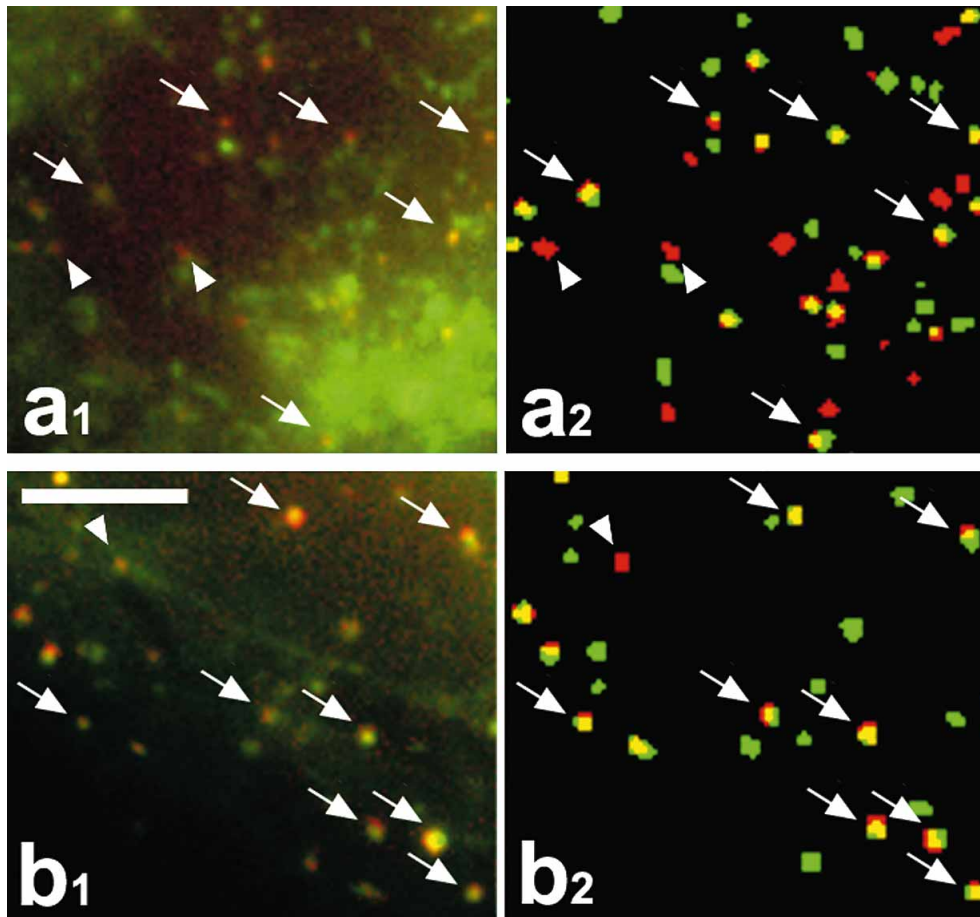


**Figure 3: The deletion mutant  $\Delta$ cys-hCgB-EYFP is efficiently transported in both basolateral- and apical-like carriers.** Vero cells were cotransfected with  $\Delta$ cys-hCgB-EYFP (red) and GPI-ECFP (green) ( $a_1$ ,  $a_2$ ) or VSVG-ECFP (green) ( $b_1$ ,  $b_2$ ) and treated as described (see Methods). Colocalization of respective signals, indicated by yellow, was analyzed as described (see Methods). Note that arrows indicate representative colocalizing signals and arrowheads representative non-colocalizing  $\Delta$ cys-hCgB-EYFP signals. Scale bar, 5  $\mu$ m.

To exclude the possibility that the ectopic expression of a membrane protein specific for basolateral- or apical-like carriers may boost the formation of the respective carriers, thereby effecting the selective sorting of secretory proteins, we analyzed whether the targeting of hCgB-EYFP remains selective if both carrier types are available in similar proportions. We achieved this by triple transfection experiments with VSVG-ECFP, GPI-EYFP and hCgBmyc or  $\Delta$ cys-hCgBmyc. These experiments confirmed a dominant packaging of hCgBmyc into basolateral-like carriers, whereas its loop-deleted equivalent entered both pathways with the same efficiency (not shown). Even in cells featuring an excess of apical-like carriers, the selective packaging of hCgBmyc into basolateral-like carriers was still evident (not shown), indicating that its transport selectivity is largely unaffected by the ratio of basolateral- and apical-like carriers. In contrast, the partition of  $\Delta$ cys-hCgBmyc in both carrier-types was seemingly dependent on their ratio (not shown) and thus consistent with nonselective (bulk) transport.

The nonselective transport of  $\Delta$ cys-hCgB-EYFP in basolateral- and apical-like carriers of Vero cells raised the question as to whether it is also secreted nonselectively in polarized epithelial cells. We therefore analyzed the secretion of a similar fusion protein,  $\Delta$ cys-hCgBmyc, using filter-grown, stably transfected MDCK cells and radioactive pulse-chase labeling. Strikingly,  $42.2\% \pm 12.4$  SD and  $57.8\% \pm 12.4$  SD ( $n = 3$  independent experiments) of the fusion protein were secreted into the basolateral and apical medium, respectively. The abundant apical secretion of  $\Delta$ cys-hCgBmyc is consistent with the value of 60.4% found for the colocalization of  $\Delta$ cys-hCgB-EYFP and GPI-ECFP in Vero cells. The secretion of  $\Delta$ cys-hCgBmyc into the basolateral medium of MDCK cells was less pronounced as compared to the value of colocalization between  $\Delta$ cys-hCgB-EYFP and VSVG-ECFP found in Vero cells (see Discussion). Collectively, our findings show that the deletion of a 20 amino acid N-terminal loop-structure of hCgB-EYFP overrides its transport selectivity in nonepithelial as well as epithelial cells.

**The biogenesis of basolateral- and apical-like carriers is characterized by distinct Golgi-topologies**

How does the TGN, as a central sorting station of the secretory pathway, accomplish the biogenesis of different types of carriers? We have approached this question by examining the packaging of soluble hCgB-EYFP into basolateral-like carriers during their biogenesis. Consistent with their extensive cotransport, hCgB-EYFP (red) and VSVG-ECFP (green) were frequently observed in the same vesicular/tubular extensions of the Golgi as revealed by 3D microscopy following deconvolution (Figure 4a,b, arrows). With live-cell, dual-color imaging, such extensions were seen to emanate from the donor membrane and occasionally displayed bud-formation at the tip (Figure 4g,h<sub>2</sub>). It is possible that membrane fission at different positions along these tubular extensions may result in the formation of carriers with varied elongated morphologies (see below). In contrast, hCgB-EYFP (red) was largely excluded from vesicular/tubular extensions of the Golgi where apical-like carriers containing GPI-ECFP (green) exited (Figure 4c,d, arrowheads). The pronounced cotransport of  $\Delta$ cys-

hCgB-EYFP with GPI-ECFP permitted monitoring of the packaging of soluble cargo into apical-like carriers. Interestingly, the vast majority of visible extensions at the Golgi positive for GPI-ECFP displayed a spherical appearance (Figure 4e,f, arrows). This was in contrast to the frequently observed elongated Golgi protrusions giving rise to basolateral-like carriers which on average were approximately twice as long (Figure 4a,b). Together, these data show copackaging of the secretory marker hCgB-EYFP with the membrane marker VSVG-ECFP into the same basolateral-like carrier. The segregation of secretory hCgB-EYFP and the membrane marker GPI-ECFP at the Golgi observed here is in agreement with the finding that the separation of apical and basolateral membrane markers occurs in the same compartment (19).

**Secretory and membrane cargo is segregated in basolateral-like carriers**

Employing dual-color, live-cell imaging, our studies showed that basolateral-like carriers displayed a pleiomorphic vesicular/tubular structure with an apparent shift of VSVG-

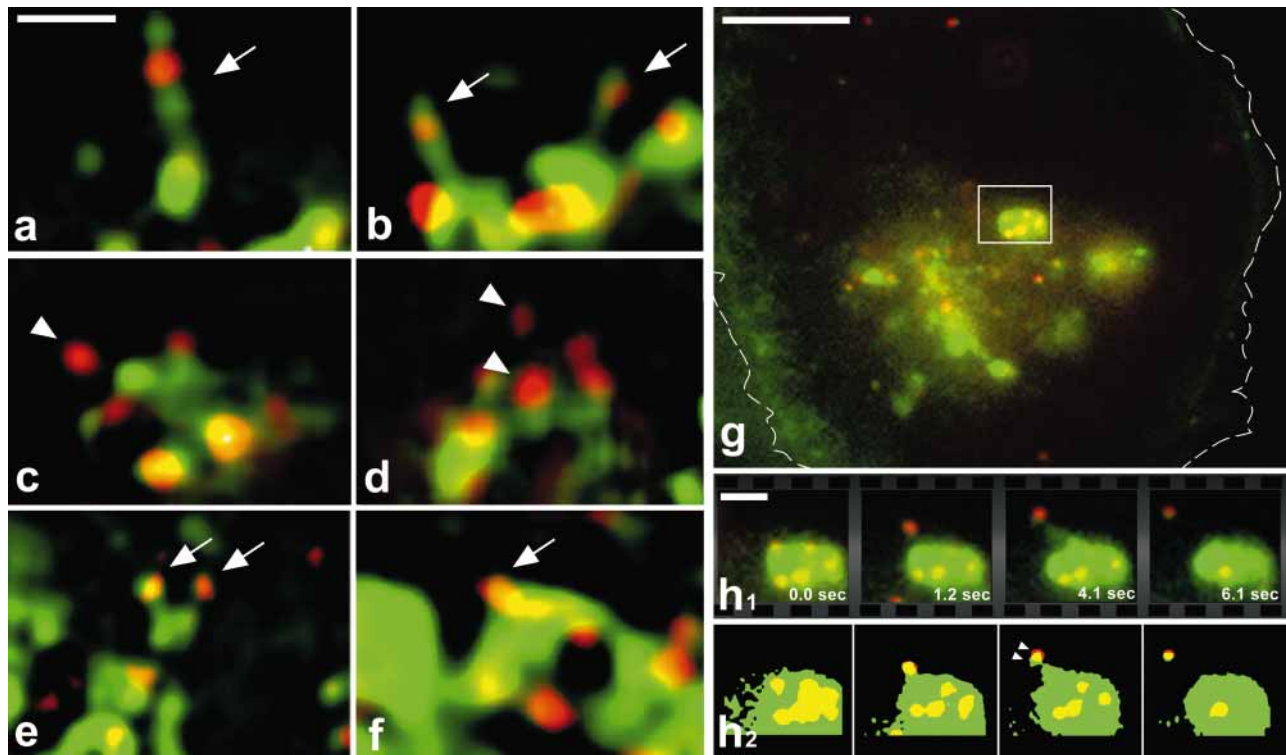


**Figure 4: Packaging of secretory cargo at the Golgi into basolateral- and apical-like carriers.** Vero cells were cotransfected with hCgB-EYFP and VSVG-ECFP (a, b, g–h<sub>2</sub>), hCgB-EYFP and GPI-ECFP (c, d), or  $\Delta$ cys-hCgB-EYFP and GPI-ECFP (e, f). (a–f) Cells were fixed and subjected to 3D dual-color fluorescence microscopy. The 3D stacks obtained were deconvolved. Single deconvolved sections show tubular extensions of the Golgi (a, b, arrows) that contain VSVG-ECFP (green) and hCgB-EYFP (red). Single deconvolved sections show that in the periphery of the Golgi, hCgB-EYFP (red) and GPI-ECFP (green) do not colocalize (c, d, arrowheads). Single deconvolved sections show the colocalization of  $\Delta$ cys-hCgB-EYFP (red) and GPI-ECFP (green) in spherical buds of the Golgi (e, f, arrows). (g–h<sub>2</sub>) Double-transfected cells were analyzed by dual-color, live-cell imaging. A single frame of a video sequence depicting the entire cell is shown (g). The dashed line indicates the cell border. For the boxed area, four selected frames of the processed dual-color video sequence are shown, depicting the formation of a Golgi-derived transport carrier (h<sub>1</sub>). The timepoints of image acquisition are indicated. Threshold-dependent image processing elucidates copackaging of both markers during bud formation (h<sub>2</sub>). Note that in the bud the fluorescence signals are displaced with respect to one another (arrowheads in h<sub>2</sub>). Scale bars: (a–f, h<sub>1</sub>, h<sub>2</sub>), 800 nm; (g), 3  $\mu$ m.

ECFP and hCgB-EYFP signals (Figure 5a,b). Frequently, double-spherical structures were detected (Figure 5a,b). Rarely, longer carriers displaying alternating VSVG-ECFP and hCgB-EYFP signals were observed (Figure 5e,f). The longer carriers, also present in the cell periphery (Figure 5e, broken line indicates the cell border), appeared to be highly dynamic, as illustrated by the image sequence in

Figure 5f. To exclude the possibility that the observed double-spherical structures consist of more than one carrier, a more detailed analysis was performed. First, a comparison of corresponding single-channel recordings (Figure 5a,b) revealed that the fluorescence signal of the VSVG-ECFP (Figure 5a,b, top right) membrane marker has a comet-like appearance with its tail (Figure 5a,b, top

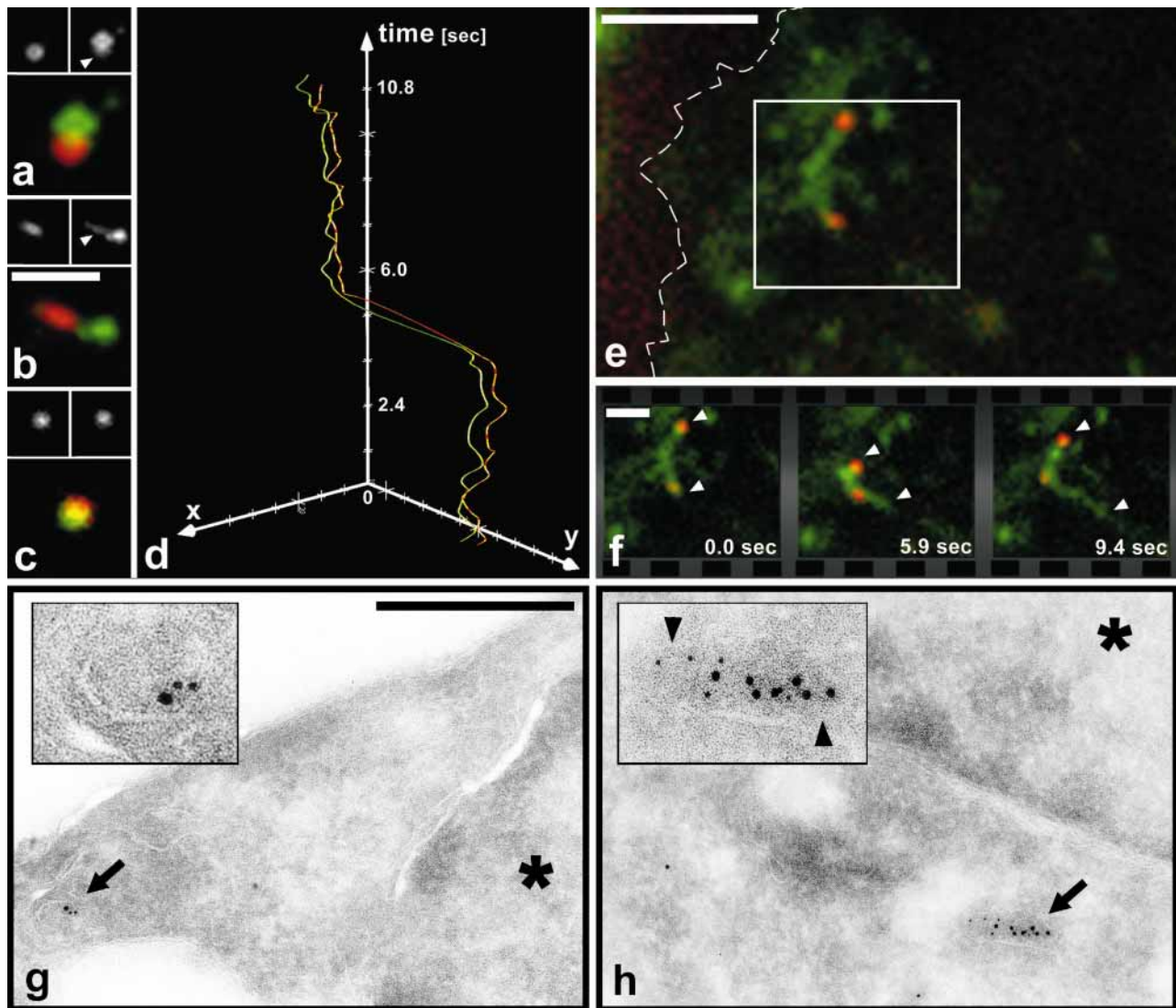


**Figure 5:** Golgi-derived basolateral-like carriers displayed distinct morphology and dynamics. (a–f) Vero cells were cotransfected with hCgB-EYFP and VSVG-ECFP (a, b, d–f), or with hCgB-ECFP (c). Cells were analyzed either directly (a, c–f) or after fixation (b) by fluorescence microscopy. Single-channel recordings of hCgB-EYFP (a–c, top left), and VSVG-ECFP (a, b, top right) and hCgB-ECFP (c, top right) are shown. Note that the fluorescence signal of the VSVG-ECFP membrane marker has a comet-like appearance with its tail (a, b arrowheads) overlapping with the hCgB-EYFP fluorescence signal. A track display obtained by automated tracking of both fluorescence signals corresponding to the double-spherical structure in (a) is shown in (d). A selected frame of a video sequence depicting the periphery of a Vero cell is shown in (e). The broken line indicates the cell border. For the boxed area in (e), three selected frames of the video sequence are shown. The time points of image acquisition are indicated. Arrowheads indicate the apparent endings of the tubular carrier. (g, h) Vero cells were cotransfected with hCgB-EYFP and untagged VSVG and processed for double-immuno electron microscopy (10 nm gold, VSVG-ECFP; 5 nm gold, hCgB-EYFP). Note that the labeled tubular structures (h, arrow and insert) were rarely detectable, whereas double-labeled spherical structures (g, arrow and insert) were frequently observed. Arrowheads in (h) indicate apparent cargo segregation. Asterisks (g, h) indicate the nucleus. Scale bars: (a–c, e, f), 800 nm; (g, h), 4  $\mu$ m. An entire movie corresponding to (f) can be viewed in the video gallery at the Traffic web site at [www.traffic.dk](http://www.traffic.dk).

right, arrowheads) overlapping with the hCgB-EYFP (Figure 5a,b, top left) fluorescence signal. Notably, this feature was not created by sequential image acquisition since it was also observed when fixed cells were analyzed (Figure 5b), but was absent in cells cotransfected with two variants of the soluble marker protein, hCgB-EYFP and hCgB-ECFP (Figure 5c). Second, automated tracking of both fluorescence signals showed a concerted movement even during extreme changes of speed and direction (Figure 5d). Third, the presence of both markers in a single carrier was confirmed by double-immuno-electron microscopy. To demonstrate this, Vero cells cotransfected with hCgB-EYFP and untagged VSVG were immunogold labeled employing antisera against EYFP (small gold particles) and VSVG (large gold particles) (Figure 5g,h). The results obtained show a specific double-labeling of distinct spherical or tubular structures (Figure 5g,h, arrows and inserts). It is interesting to note that at the ultrastructural level the segregation of soluble and membrane cargo could also be detected (Figure 5h, arrowheads).

To address whether cargo segregation was a unique feature of the basolateral secretion pathway, we analyzed cells cotransfected with GPI-ECFP and  $\Delta$ cys-hCgB-EYFP already shown to efficiently enter apical-like carriers. Strikingly, in most cases the signals of both markers appeared spherical (Figure 6a, top panel) and overlapped nearly completely (Fig-

ure 6a, lower panel, arrow). This finding is in contrast to the detected shift of signals in basolateral-like carriers containing hCgB-EYFP and VSVG-ECFP. To exclude the possibility that the lack of cargo segregation in apical-like carriers is due to the  $\Delta$ cys-hCgB-EYFP deletion mutant itself, we expressed it together with VSVG-ECFP. As for the nonmutated hCgB-EYFP, under these conditions the segregation of cargo in basolateral-like vesicles became apparent (Figure 6b, lower panel, arrowheads). The fact that basolateral- and apical-like carriers containing the same secretory cargo display a different morphology indicates that both carrier types feature unique characteristics.

**Basolateral- and apical-like carriers display differences in transport dynamics**

The track displays of basolateral- and apical-like carriers obtained by automated analysis of their transport dynamics in double-transfected Vero cells (Figures 1c and 2c) revealed an interesting feature of both carrier types. For those carriers transporting hCgB-EYFP and/or VSVG-ECFP, long-range transport was frequently observed (Figures 1c and 2c, barbed arrowheads). By contrast, for carriers transporting GPI-ECFP, short-range transport prevailed (Figure 2c, green trajectories). A quantitative analysis revealed that the maximum path-length of basolateral-like carriers containing hCgB-EYFP and VSVG-ECFP was  $1.89 \pm 0.47$  SD ( $n = 9$  cells from 3 independent experiments) times as long as observed for apical

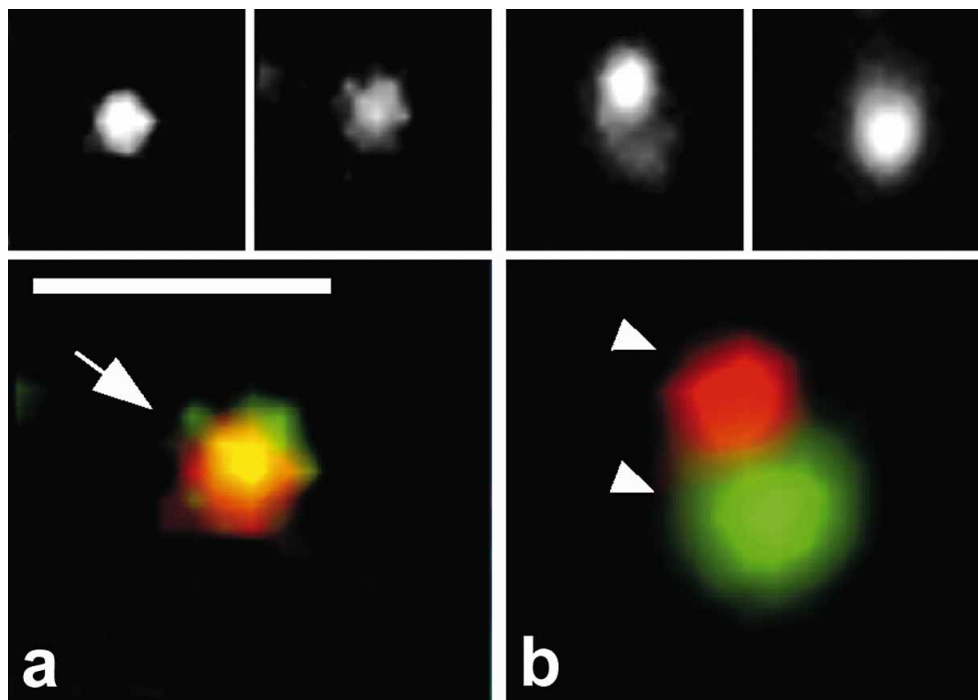


**Figure 6: Basolateral- and apical-like carriers show morphological differences.** Vero cells were cotransfected with  $\Delta$ cys-hCgB-EYFP and GPI-ECFP (a) or VSVG-ECFP (b) and fixed. Single channel recordings (top panels) as well as corresponding overlays (bottom panels) of representative carriers for both conditions are shown. Basolateral-like carriers display double-spherical structures with apparent segregation of  $\Delta$ cys-hCgB-EYFP (red) and VSVG-ECFP (green) fluorescence signals (b, arrowheads). Apical-like carriers containing  $\Delta$ cys-hCgB-EYFP and GPI-ECFP display predominantly spherical structures with overlapping signals (a, arrow). Note that yellow indicates colocalization. Scale bar, 800  $\mu$ m.

carriers containing GPI-ECFP. This finding indicates unique features of the transport machineries involved in translocation of the respective carriers.

## Discussion

Using dual-color imaging, we were able to show that nonepithelial cells are capable of packaging and transporting secretory cargo selectively in distinct types of Golgi-derived carriers. A comparison of these data with our biochemical studies on polarized MDCK cells yielded similarities between the sorting machineries of nonepithelial and epithelial cells. In both cell systems, fusion proteins of the soluble secretory marker hCgB were secreted predominantly via the basolateral/basolateral-like pathway. Furthermore, in both cases a 20-amino acid loop structure of this marker protein was crucial for selective basolateral/basolateral-like targeting. Since it has been shown that the loop structure in neuroendocrine cells mediates membrane binding in the TGN (17) and its disruption has no influence on the aggregative properties of hCgB (21), it is conceivable that membrane binding of similar motifs may also play an important role in the targeting of secretory proteins to constitutive carriers.

Employing live-cell imaging of nonepithelial cells, we analyzed the trafficking of soluble cargo in two distinct carrier types characterized by two fluorescent membrane markers. However, it is possible that parallel pathways of protein secretion involving distinct carrier subtypes, not visualized in our experiments, may exist in nonepithelial cells. Our biochemical studies of the polarized secretion of hCgB-GFP(S65T) in epithelial cells also do not allow conclusions about parallel secretion pathways. In this respect, it is interesting to note that secretory and membrane cargo are transported in distinct carriers to the sinusoidal (basolateral) plasma membrane in hepatocytes (10). This may indicate parallel routes to at least the basolateral surface of polarized epithelial cells, although in the aforementioned biochemical study, fragmentation of vesicular/tubular carriers during subcellular fractionation resulting in artificial carrier subtypes cannot be excluded. Given that similarities between the secretory pathways of epithelial and nonepithelial cells exist, further exploration of this issue in both cell systems by high-resolution multicolor imaging using additional marker proteins seems warranted.

Our study revealed that in double-transfection experiments,  $\Delta$ cys-hCgB-EYFP efficiently entered apical-like carriers positive for GPI-ECFP. On the other hand,  $\Delta$ cys-hCgB-EYFP massively colocalized with the basolateral-like marker protein VSVG-ECFP which seemingly conflicts with its competence to enter apical-like carriers. These findings suggest that the apical-like pathway of nonepithelial Vero cells, at least under our experimental conditions, is less pronounced as compared to the basolateral pathway resulting in e.g. a low synthesis rate of the respective carriers. However, the machinery to generate apical-like carriers seems to be functional and may be utilized by suited exogenous proteins like GPI-ECFP or

under special physiological conditions such as cell migration. This assumption reflects previous suggestions concerning the apical-like pathway of other nonepithelial cell lines (14). Therefore, it is important to note that exogenously expressed proteins may affect the balance of membrane traffic in the secretory pathway.

Our dual-color imaging approach revealed three main differences of the apical- and basolateral-like pathway. First, we found distinct Golgi morphologies during biogenesis of basolateral- and apical-like carriers. Basolateral-like carriers derived from tubular extensions of the Golgi, whereas apical-like carriers formed predominantly at spherical buds. These differences may reflect the different machineries involved in carrier biogenesis. In this context, it is tempting to speculate that these differences are linked, e.g. to the recently described CtBP/BARS enzymatic activity involved in membrane fission of Golgi tubular networks (22) or to the action of different isoforms of dynamin shown to be located at the TGN (23,24). Second, we observed that the differences in apical- and basolateral-like carrier biogenesis at the level of the Golgi was mirrored by the morphology of the respective carriers. Whereas basolateral carriers displayed a vesicular/tubular morphology with apparent cargo segregation, apical-like carriers appeared spherical with overlapping signals for both cargo proteins. Thus, the cargo segregation observed for basolateral-like carriers may reflect the existence of distinct subdomains within a given carrier, as has been recently postulated (25,26). Third, we found that basolateral- and apical-like carriers displayed a different pattern of movement. These data suggest that different transport mechanisms may be utilized for the respective apical- and basolateral-like secretion pathways. Therefore, it is conceivable that nonepithelial cells regulate and direct protein secretion by controlling the trafficking of respective transport carriers. A differential regulation of protein secretion would enable these cells to respond properly to transient polarization events as they occur, e.g. during cell migration.

## Materials and Methods

### Plasmid construction

Human chromogranin B-enhanced yellow fluorescent protein plasmid was generated from pCDM8-hCgB(S65T) (20) by restriction with HindIII/KpnI and ligation of the obtained hCgB cDNA fragment into pEYFP-N1 (Clontech, Palo Alto, CA, USA), opened with corresponding restriction enzymes. The  $\Delta$ cys-hCgB-EYFP plasmid was generated by exchanging the XhoI/NotI-fragment of pCDM8- $\Delta$ cys-hCgBmyc (27) with the XhoI/NotI-fragment of hCgB-EYFP-N1 (16). The HindIII/NotI fragment of the obtained vector was subcloned into pcDNA3 (Invitrogen, Karlsruhe, Germany) opened at the respective restriction sites. pRc/CMV-hCgBmyc and pRc/CMV- $\Delta$ cys-hCgBmyc are identical with previously described constructs (27). VSVG-ECFP is identical with previously described VSVG3-SP-ECFP (19). GPI-ECFP is identical with previously described CFP-GL-GPI (19), except that a different downstream primer (5'-GCTGATCATACTTGTCAGCTCGTCC-3') was used for the final polymerase chain reaction (PCR). This resulted in the absence of the N-glycosylation site present in GFP-GL-GPI. GPI-ECFP was sorted apically in MDCK cells to a very similar extent as compared to GFP-GL-GPI (P.K., unpublished data).

### Expression of recombinant proteins

Using electroporation, Vero cells were transiently double-transfected, either with plasmids encoding for hCgB-EYFP/ $\Delta$ cys-hCgB-EYFP and VSVG-ECFP or with GPI-ECFP, and plated on LabTek coated 4-chambered cover glasses (Nalge Nunc International, Wiesbaden, Germany) (16). Cells transfected with cDNAs encoding for hCgB-EYFP/ $\Delta$ cys-hCgB-EYFP and VSVG-ECFP were incubated for 24 h at 40°C and 5% CO<sub>2</sub> in cell culture medium (EMEM supplemented with 10% fetal calf serum and 2 mM glutamine). During the last 12 h of incubation, 2 mM sodium butyrate was present. After replacement of culture medium by block medium (culture medium supplemented with 10 mM HEPES-KOH, pH 7.4), cells were incubated for 2 h at 20°C in the presence of cycloheximide (10  $\mu$ g ml<sup>-1</sup>). Cells transfected with cDNAs encoding for hCgB-EYFP/ $\Delta$ cys-hCgB-EYFP and GPI-ECFP were incubated for 24 h at 37°C. The culture medium was then replaced by block medium supplemented with cycloheximide (10  $\mu$ g ml<sup>-1</sup>) and cells were incubated for 1.5 h at 20°C. Thereafter, 2 units PI-PLC (Glyko, Inc., Novato, USA) were added and cells were incubated for an additional 30 min at 20°C. Vero cells were triple-transfected with cDNAs encoding for VSVG-ECFP, GPI-EYFP and hCgBmyc or  $\Delta$ cys-hCgBmyc and were incubated for 24 h at 37°C and 5% CO<sub>2</sub>. After replacement of culture medium by block medium supplemented with cycloheximide (10  $\mu$ g ml<sup>-1</sup>) cells were incubated for 2 h at 20°C, then for 30 min at 37°C and subsequently fixed. In the case of GPI-ECFP expression, PI-PLC-treatment was carried out prior to fixation.

MDCK cells (strain II) were cultured as described (28). Cells were transfected with cDNAs encoding for hCgB-GFP(S65T) (20) or  $\Delta$ cys-hCgBmyc using lipofectAMINE (Life Technologies, Inc., Rockville, MD, USA) according to the supplier's instructions. Forty-eight hours after transfection, cells were incubated in culture medium supplemented with G418 (0.5 mg ml<sup>-1</sup>) and selected for 3 weeks before use.

### Pulse-chase analysis

In order to study the polarized secretion of hCgB-GFP(S65T) or  $\Delta$ cys-hCgBmyc, stable transfected MDCK cell lines were grown on 75 mm diameter Transwell-Filters (Costar, Corning, NY, USA) for 5–7 days. Media were changed every 24 h. Expression of hCgB-GFP(S65T) or  $\Delta$ cys-hCgBmyc was induced by incubation of cells in culture medium containing 10 mM sodium butyrate for 21 h. Thereafter, cells were incubated for 30 min in sulfate-free medium (25). During the same incubation period, the integrity of the cell monolayer was assessed by monitoring the diffusion of [<sup>14</sup>C]sucrose (615 mCi mmol<sup>-1</sup>, Amersham, Uppsala, Sweden) from the apical to the basolateral compartment of the chamber. Under these conditions, less than 0.5% of the labeled sucrose was recovered from the basolateral medium. Cells were then labeled for 3 h from the apical side with 10 ml pulse medium containing 2–3 mCi ml<sup>-1</sup> of carrier-free [<sup>35</sup>S]sulfate (Amersham) to specifically label proteins in the TGN (29).

After pulse labeling, media were collected and concentrated by ultrafiltration (Centriprep, Millipore, Bedford, MA, USA). Equal aliquots of concentrated media were analyzed for secretion of proteins either directly (endogenous gp80) or by immunoprecipitation with the polyclonal D2-antiserum against hCgB-GFP(S65T) as described (15) or ascites antibody 9E10 against the myc epitope of  $\Delta$ cys-hCgB-myc, followed by SDS-PAGE and phosphoimaging. Under these conditions, the endogenous gp80 was secreted mainly at the apical side of the cells ( $\geq$  79%) as previously reported (30).

### Dual-color imaging and image analysis

Dual-color imaging of single cellular sections and automated image analysis were performed as described (16,31). For every image sequence, 60 consecutive frame pairs (each consisting of 2 single channel recordings) were acquired at a rate of 3–5 frame pairs s<sup>-1</sup>. For automated image analysis, regions of interest (ROIs) displaying a low and even cellular back-

ground were selected. The ROIs were subjected to automated object detection resulting in binary image sequences. Automated tracking of the binary image sequences yielded the trajectories of detected objects. These were visualized in three-dimensional reconstructions with time evolving along the z-axis. Automated analysis of colocalization over time (referred to here as dynamic colocalization) was determined by the continuous trajectory reconstructions (16). For manual image analysis, image sequences showing the entire cell were analyzed by comparison of selective frame pairs with IP-lab software 3.2.2 (Scanalytics, Fairfax, VA, USA). Because the accuracy of automated evaluation critically depends on signal-to-noise ratio and object density, it results in values 10–15% lower as compared to manual analysis. Manual analysis is limited to the evaluation of selected, corresponding frame pairs, i.e. the analysis of static images. Thus, manually obtained values are artificially increased by random colocalization. In order to compensate for the errors of automated and manual analysis, their values were averaged. For dual-color 3D imaging of fixed cells, 90 sections per cell were acquired with a step width of 100 nm using a piezo z-stepper (Physik Instrumente GmbH & Co., Palmach, Germany). 3D stacks were processed by using the deconvolution extension of TILLvisION (T.I.L.L. Photonics GmbH, Gräfelling, Germany). Threshold-based image processing was performed by the 'Trace Contour' filter of Adobe Photoshop 5.5 (Adobe Systems, Inc.). The obtained processed image data were verified by 'line profile' analysis with TILLvisION (data not shown).

### Electron microscopy

For immunogold electron microscopy, Vero cells double-transfected with cDNAs encoding for hCgB-EYFP and untagged VSVG were incubated for 2 h at 20°C followed by 15 min incubation at 37°C. Thereafter, cells were fixed (4% paraformaldehyde, 0.2% glutaraldehyde). Ultrathin cryosections (80 nm) were prepared as described (32). Double-immunolabeling was performed according to Slot et al. (33). In brief: cells were first incubated with rabbit anti-GFP serum (1 : 300, Molecular Probes, A-11122) followed by labeling with 5 nm protein A-gold. Subsequently, cells were incubated with 8% paraformaldehyde to denature the protein A (5 nm gold)-free antibodies bound to EYFP. Cells were then incubated with rabbit anti-VSVG serum (34) (1 : 100) followed by labeling with 10 nm protein A-gold.

## Acknowledgments

We are indebted to Paul Verkade, and in particular to Andrea Hellwig, for their help with electron microscopy, and to Alan Summerfield for his help with photography. We would like to acknowledge the generous gift of 9E10 ascites antibody by E. Karsenti. We thank Jacqueline Trotter for critical comments on the manuscript and W.B. Huttner for continuous support. We gratefully acknowledge Olympus and T.I.L.L. Photonics for generously providing equipment and support for the Imaging Center at the Department of Neurobiology, Heidelberg. Amin Rustom and Mark Bajohrs were supported by the Landesgraduierstipendium Baden-Württemberg. H.-H. Gerdes was the recipient of a grant from the Deutsche Forschungsgemeinschaft (SFB 488/B2) and a Fond der Chemischen Industrie.

## References

- Griffiths G, Simons K. The trans-Golgi network: sorting at the exit site of the Golgi complex. *Science* 1986;234:438–443.
- Rodriguez-Boulan E, Nelson WJ. Morphogenesis of the polarized epithelial cell phenotype. *Science* 1989;245:718–725.
- Rindler MJ, Ivanov IE, Plesken H, Rodriguez-Boulan E, Sabatini DD. Viral glycoproteins destined for apical or basolateral plasma membrane domains traverse the same Golgi apparatus during their intracellular transport in doubly infected Madin-Darby canine kidney cells. *J Cell Biol* 1984;98:1304–1319.

4. Wandinger-Ness A, Bennett MK, Antony C, Simons K. Distinct transport vesicles mediate the delivery of plasma membrane proteins to the apical and basolateral domains of MDCK cells. *J Cell Biol* 1990;111:987–1000.
5. Lisanti MP, Caras IW, Davitz MA, Rodriguez-Boulan E. A glycopospholipid membrane anchor acts as an apical targeting signal in polarized epithelial cells. *J Cell Biol* 1989;109:2145–2156.
6. Keller P, Simons K. Post-Golgi biosynthetic trafficking. *J Cell Sci* 1997;110:3001–3009.
7. Fölsch H, Ohno H, Bonifacino JS, Mellman I. A novel clathrin adaptor complex mediates basolateral targeting in polarized epithelial cells. *Cell* 1999;99:189–198.
8. Mostov KE, Verges M, Altschuler Y. Membrane traffic in polarized epithelial cells. *Curr Opin Cell Biol* 2000;12:483–490.
9. Caplan MJ, Stow JL, Newman AP, Madri J, Anderson HC, Farquhar MG, Palade GE, Jamieson JD. Dependence on pH of polarized sorting of secreted proteins. *Nature* 1987;329:632–635.
10. Saucan L, Palade GE. Membrane and secretory proteins are transported from the Golgi complex to the sinusoidal plasmalemma of hepatocytes by distinct vesicular carriers. *J Cell Biol* 1994;125:733–741.
11. Scheiffele P, Peranen J, Simons K. N-glycans as apical sorting signals in epithelial cells. *Nature* 1995;378:96–98.
12. Rodriguez-Boulan E, Gonzalez A. Glycans in post-Golgi apical targeting: sorting signals or structural props? *Trends Cell Biol* 1999;9:291–294.
13. Yoshimori T, Keller P, Roth MG, Simons K. Different biosynthetic transport routes to the plasma membrane in BHK and CHO cells. *J Cell Biol* 1996;133:247–256.
14. Müsch A, Xu H, Shields D, Rodriguez-Boulan E. Transport of vesicular stomatitis virus G protein to the cell surface is signal mediated in polarized and nonpolarized cells. *J Cell Biol* 1996;133:543–558.
15. Wacker I, Kaether C, Kromer A, Migala A, Almers W, Gerdes HH. Microtubule-dependent transport of secretory vesicles visualized in real time with a GFP-tagged secretory protein. *J Cell Sci* 1997;110:1453–1463.
16. Rustom A, Gerlich D, Rudolf R, Heinemann C, Eils R, Gerdes HH. Analysis of fast dynamic processes in living cells: high-resolution and high-speed dual-color imaging combined with automated image analysis. *Biotechniques* 2000;28:722–728.
17. Glombik MM, Krömer A, Salm T, Huttner WB, Gerdes HH. The disulfide-bonded loop of chromogranin B mediates membrane binding and directs sorting from the trans-Golgi network to secretory granules. *EMBO J* 1999;18:1059–1070.
18. Huttner WB, Gerdes H-H, Rosa P. The granin (chromogranin/secretogranin) family. *Trends Biochem Sci* 1991;16:27–30.
19. Keller P, Toomre D, Díaz E, White J, Simons K. Multicolour imaging of post-Golgi sorting and trafficking in live cells. *Nat Cell Biol* 2001;3:140–149.
20. Kaether C, Gerdes H-H. Monitoring of protein secretion with green fluorescent protein. *Meth Enzymol* 1999;302:11–19.
21. Chant E, Weiss U, Huttner WB. The disulfide bond in chromogranin B, which is essential for its sorting to secretory granules, is not required for its aggregation in the trans-Golgi network. *FEBS Lett* 1994;351:225–230.
22. Weigert R, Silletta MG, Spano S, Turacchio G, Cericola C, Colanzi A, Senatore S, Mancini R, Polishchuk EV, Salmons M, Facchiano F, Burger KN, Mironov A, Luini A, Corda D. CtBP/BARS induces fission of Golgi membranes by acylating lysophosphatidic acid. *Nature* 1999;402:429–433.
23. Jones SM, Howell KE, Henley JR, Cao H, McNiven MA. Role of dynamin in the formation of transport vesicles from the trans-Golgi network. *Science* 1998;279:573–577.
24. Kreitzer G, Marmorstein A, Okamoto P, Vallee R, Rodriguez-Boulan E. Kinesin and dynamin are required for post-Golgi transport of a plasma-membrane protein. *Nat Cell Biol* 2000;2:125–127.
25. Röper K, Corbeil D, Huttner WB. Retention of prominin in microvilli reveals distinct cholesterol-based lipid micro-domains in the apical plasma membrane. *Nat Cell Biol* 2000;2:582–592.
26. Stephens DJ, Lin-Marq N, Pagano A, Pepperkok R, Paccard J. COPI-coated ER-to-Golgi transport complexes segregate from COPII in close proximity to ER exit sites. *J Cell Sci* 2000;113:2177–2185.
27. Krömer A, Glombik MM, Huttner WB, Gerdes H-H. Essential role of the disulfide-bonded loop of chromogranin B for sorting to secretory granules is revealed by expression of a deletion mutant in the absence of endogenous granin synthesis. *J Cell Biol* 1998;140:1331–1346.
28. Corbeil D, Röper K, Hannah MJ, Hellwig A, Huttner WB. Selective localization of the polytopic membrane protein prominin in microvilli of epithelial cells – a combination of apical sorting and retention in plasma membrane protrusions. *J Cell Sci* 1999;112:1023–1033.
29. Huttner WB. Tyrosine sulfation and the secretory pathway. *Annu Rev Physiol* 1988;50:363–376.
30. Urban J, Parczyk K, Leutz A, Kayne M, Kondor-Koch C. Constitutive apical secretion of an 80-kD sulfated glycoprotein complex in the polarized epithelial Madin-Darby canine kidney cell line. *J Cell Biol* 1987;105:2735–2743.
31. Tvaruskó, W, Bentele M, Mistele T, Rudolf R, Kaether C, Spector DL, Gerdes HH, Eils R. Time-resolved analysis and visualization of dynamic processes in living cells. *Proc Natl Acad Sci USA* 1999;96:7950–7955.
32. Aaku-Saraste E, Oback B, Hellwig A, Huttner WB. Neuroepithelial cells downregulate their plasma membrane polarity prior to neural tube closure and neurogenesis. *Mech Dev* 1997;69:71–81.
33. Griffiths G. *Fine Structure Immuno-Cytochemistry*. Berlin, Heidelberg: Springer-Verlag; 1993. p. 269–270.
34. Matlin KS, Reggio H, Helenius A, Simons K. Pathway of vesicular stomatitis virus entry leading to infection. *J Mol Biol* 1982;156:609–631.